



# Development and evaluation of a high-resolution reanalysis of the East Australian Current region using the Regional Ocean Modelling System (ROMS 3.4) and Incremental Strong-Constraint 4-Dimensional Variational data assimilation (IS4D-Var)

Colette Kerry<sup>1</sup>, Brian Powell<sup>2</sup>, Moninya Roughan<sup>1</sup>, and Peter Oke<sup>3</sup>

<sup>1</sup>University of New South Wales, Sydney, NSW, 2052, Australia

<sup>2</sup>University of Hawai'i at Manoa, Honolulu, Hawaii, USA

<sup>3</sup>CSIRO Marine and Atmospheric Research, Hobart, Australia

*Correspondence to:* Colette Kerry (c.kerry@unsw.edu.au)

## Abstract.

As with other western boundary currents globally, the East Australian Current (EAC) is inherently dynamic making it a challenge to model and predict. For the EAC region, we combine a high-resolution state-of-the-art numerical ocean model with a variety of traditional and newly available observations using an advanced variational data assimilation scheme. The numerical model is configured using the Regional Ocean Modelling System (ROMS 3.4) and takes boundary forcing from the BlueLink ReANalysis (BRAN3). For the data assimilation we use an Incremental Strong-Constraint 4-Dimensional Variational (IS4D-Var) scheme. This paper describes the data assimilative model configuration that achieves an optimised minimisation of the difference between the modelled solution and the observations to give a dynamically-consistent 'best-estimate' of the ocean state over a 2-year period. The reanalysis is shown to represent both assimilated and non-assimilated observations well. It achieves mean spatially-averaged RMS residuals with the observations of 7cm for SSH and 0.4° C for SST over the assimilation period. The time-mean RMS residual for subsurface temperature measured by Argo floats is a maximum of 1° C between water depths of 100-300m and smaller throughout the rest of the water column. Velocities at several offshore and continental shelf moorings are well represented in the reanalysis with complex correlations between 0.8-1 for all observations in the upper 500m. Surface radial velocities from a high-frequency radar array are assimilated and the reanalysis provides surface velocity estimates with complex correlations with observed velocities of 0.8-1 across the radar footprint. Comparison with independent (non-assimilated) shipboard CTD cast observations shows a marked improvement in the representation of the subsurface ocean in the reanalysis, with the RMS residual in potential density reduced to about half of the residual with the free-running model in the upper eddy-influenced part of the water column. This shows that information is successfully propagated from observed variables to unobserved regions as the assimilation system uses the model dynamics to determine covariance, such that the ocean state better fits and is in balance with the observations. This is the first study to generate a reanalysis of the region at such a high resolution, making use of an unprecedented observational data set and using an assimilation method that uses the time-evolving model physics to adjust the model in a dynamically consistent way. As such, the reanalysis potentially represents



a marked improvement in our ability to capture important circulation dynamics in the EAC. The reanalysis is being used to study EAC dynamics, observation impact in state-estimation and as forcing for a variety of downscaling studies.

## 1 Introduction

The East Australian Current (EAC) is the Western Boundary Current (WBC) of the South Pacific subtropical gyre, flowing poleward along the east coast of Australia. The EAC has the weakest mean flow of the WBCs associated with the subtropical gyres (Mata et al., 2000) but its flow is characterised by high eddy variability (Mata et al., 2006) comparable with stronger WBCs such as the Gulf Stream, the Kuroshio and the Agulhas Current (e.g. Gordon et al. (1983); Feron (1995)). The EAC forms in the South Coral Sea (15-24° S) and intensifies as it flows along the coast of southeast Queensland and northern New South Wales (NSW) (22-35° S) – refer to Figure 1 for geographical location. The current strengthens dramatically as the continental shelf narrows to 15 km at its narrowest point (31° S) and typically separates from the coast between 31-33° S (Cetina Heredia et al., 2014). Turning eastward to form the Tasman Front, the current sheds large warm- and cold-core eddies in the Tasman Sea every 90-110 days (Oke and Middleton, 2000; Cetina Heredia et al., 2014). The high eddy variability makes the EAC a challenging system to observe and predict.

In general, the kinetic energy of the ocean is dominated by mesoscale eddies that fluctuate on time scales of days to months and on spatial scales of tens to 100s of kilometers and exceeds the mean flow by an order of magnitude or more (Stammer, 1997; Ferrari and Wunsch, 2009). Eddies are typically generated due to barotropic or baroclinic instabilities which are unpredictable so effective state-estimation and prediction of the mesoscale circulation requires data assimilation techniques that combine ocean observations with a dynamical model. Much of the effort towards data assimilative modelling of the EAC region has been as part of the development Australia's Bluelink ocean data assimilation system (BODAS) (Oke et al., 2005, 2008, 2013) which uses an Ensemble Optimal Interpolation (EnOI) based scheme. The BODAS has been a useful and relatively efficient method to provide ocean state estimates of the Australian region. EnOI uses long-run statistics to generate the covariance of model points and assimilates observations at a single time to generate adjusted initial conditions for each assimilation window.

In this work we use 4-dimensional variational data assimilation (4D-Var), which adjusts the model initial conditions, boundary and surface forcings such that the difference between the model solution of the time-evolving flow and all available observations is minimised over an assimilation interval. A major advantage of the 4D-Var scheme is that it uses the linearised model equations and their adjoint to compute covariances, so the model is adjusted in a dynamically consistent way to minimise the difference between the observations and the modelled time-evolving ocean state. Using the linearised equations allows dynamical connections between state variables to propagate information from observed variables to unobserved, dynamically-linked variables without requiring ensemble or long-run statistics. The state estimate is a solution of the model equations, and the minimisation process can be used to understand the sensitivity of the ocean circulation (e.g. Moore et al. (2009); Powell et al. (2012)). Zavala-Garay et al. (2012) used 4D-Var with ROMS to assimilate Sea Surface Height (SSH), Sea Surface Temperature (SST) and Expendable Bathythermograph (XBT) observations into a coarse resolution (18-30km) model of the EAC



region, and use an empirical relationship between surface and subsurface properties to help propagate the dominant surface observations to the subsurface and improve their subsurface estimates.

Combining a state-of-the-art numerical ocean model with a variety of traditional and newly available observations, we generate a high resolution ocean state estimate of the EAC region over a 2-year period (Jan 2012 - Dec 2013). This paper describes the development and evaluation of the data assimilative model configuration. We begin by configuring a numerical model of the EAC region that is capable of representing the mean ocean circulation and its eddy variability. The model is configured to resolve the continental shelf which is 15km wide at its narrowest point and may be important in accelerating the EAC and driving the current's separation (Oke and Middleton, 2000). In order to correctly represent the spatial and temporal evolution of the eddy field, we need to constrain the model with observations. We configure a 4D-Var data assimilation system that reduces the difference between the model solution and observations, given prior assumptions of the uncertainties in the observations and the model background state. In addition to the traditional data streams (satellite derived SSH and SST, Argo profiling floats and XBT lines) we exploit newly available observations that were collected as part of Australia's Integrated Marine Observing System (IMOS, [www.imos.org.au](http://www.imos.org.au)). These include velocity and hydrographic observations from a deep-water mooring array and several moorings on the continental shelf, High-Frequency radar observations, and ocean gliders.

We show that the assimilation configuration developed in this work results in near-optimal minimisation of the differences between the modelled solution and the observations. As such, the reanalysis provides us with a 'best estimate' of the ocean state that is dynamically consistent within each assimilation time window. The reanalysis is being used to study the variability and separation dynamics of the EAC. Furthermore, the 4D-Var method allows us to use the reanalysis to quantify the impact of particular data streams on circulation estimates, which has the potential to provide important information for assessing and improving the observing system design. The product is also being used as boundary forcing for a variety of downscaling studies in coastal southeastern Australia. This data assimilative model represents a significant improvement on previous modelling work in the EAC for these purposes e.g. Roughan et al. (2003) which was based on climatology, Macdonald et al. (2013, 2014) which focused on process studies of warm core and cold core eddies, and Zavala-Garay et al. (2012) which used 4D-Var with a much coarser resolution.

The reanalysis development and evaluation is presented as follows. In Section 2, we describe the numerical model configuration, including validation of a 10-year free-running simulation to provide confidence that the model is correctly representing the region's circulation dynamics. In Section 3, we describe the development of the reanalysis, including the data assimilation scheme used, the assimilation configuration and the observations. The reanalysis performance is evaluated in Section 4 using a variety of metrics to illustrate the system's skill. A summary and conclusions are presented in Section 5.

## 2 Numerical Model

### 2.1 Model Configuration

We use the Regional Ocean Modeling System (ROMS, version 3.4) to simulate the eddy general circulation in the southeastern Australia oceanic region. ROMS is a free-surface, hydrostatic, primitive equation ocean model solved on a curvilinear



grid with a terrain-following vertical coordinate system (Shchepetkin and McWilliams, 2005). For computational efficiency, ROMS uses a split-explicit time-stepping scheme allowing the barotropic solution to be computed at a much smaller time step than is used for the (slow-mode) baroclinic equations using a temporal averaging filter to ensure preservation of tracers and momentum and minimise aliasing of unresolved barotropic signals into the baroclinic motions (Shchepetkin and McWilliams, 2005). The ROMS computational kernel is further described in Shchepetkin and McWilliams (1998, 2003).

Sub-grid scale horizontal mixing of momentum and tracers uses a harmonic (3-point stencil) mixing operator (Haidvogel and Beckmann, 1999), and the viscosity is derived from the horizontal divergence of the deviatoric stress tensor (Wajsovicz, 1993). The diffusion and viscosity coefficients are scaled by grid-size such that less explicit diffusion occurs in the high-resolution region than in the lower resolution region. The Mellor and Yamada (1982) level-2.5, second-moment turbulence closure scheme (MY2.5) is used in parameterising vertical turbulent mixing of momentum and tracers.

The model domain (shown in Figure 1) extends from Fraser Island in the north ( $25.25^{\circ}$  S) to below the NSW/Victoria border in the south ( $41.55^{\circ}$  S) and nearly 1000 km offshore. The northern boundary is chosen at a latitude where the EAC remains fairly coherent and is upstream of the region of elevated eddy variability (refer to Figure 2a). The grid is rotated  $20^{\circ}$  clockwise such that it is orientated predominantly along-shore in the y-dimension and cross-shore in the x-dimension. The model has a variable horizontal resolution in the cross-shore direction, with 2.5 km ( $1/44^{\circ}$ ) over the continental shelf and slope that gradually increases to 6 km ( $1/18^{\circ}$ ) in the open ocean. The horizontal resolution is 5 km ( $1/22^{\circ}$ ) in the along-shore direction. The model is configured with 30 vertical s-layers distributed with a higher resolution in the upper 500m to resolve the wind driven mesoscale circulation and near the bottom for improved resolution of the bottom boundary layer. The vertical stretching scheme of Souza et al. (2014) is used, which ensures a constant-depth surface layer to better represent satellite-derived SST, better resolve the ocean surface currents, and reduce the representation error of radio-measured surface currents. The bathymetry for the model was obtained from the 50m Multibeam Dataset for Australia from Geoscience Australia (Whiteway, 2009).

In models using terrain-following coordinate systems, steep topographic gradients generate numerical errors associated with the computation of the pressure gradient term resulting in artificial along-slope flows (Haney, 1991; Mellor et al., 1994). These errors depend on the topographic steepness and the intensity of the stratification (Haidvogel et al., 2000). The variable cross-shore resolution improves the bathymetric resolution over the continental shelf and minimises pressure gradient errors over the steep topography of the continental slope, while reducing computational expense by allowing coarser resolution in the deep ocean. ROMS is effective at minimising these horizontal pressure gradient (HPG) errors (Shchepetkin and McWilliams, 2003); although, a certain degree of topographic smoothing is usually still desirable. For this study, a smoothing method has been applied in which a high priority is placed on maintaining the width of the continental shelf and preserving the seamounts that potentially play a role in steering of the EAC, while minimising HPG errors to an acceptable level. Accurate representation of the continental shelf was considered paramount as the shelf is thought to have an important influence on the EAC (e.g. Oke and Middleton (2000)).

The model uses initial conditions and boundary forcing from the BlueLink ReANalysis version 3p5 (BRAN3) (Oke et al., 2013). BRAN is a multi-year integration of the Ocean Forecasting Australian Model (OFAM) and the Bluelink Ocean Data



Assimilation System (BODAS; Oke et al. (2008)). The boundary forcing is applied daily. The Chapman condition (Chapman, 1985) is applied to the free surface and the Flather condition (Flather, 1976) is applied to the barotropic velocity so that barotropic energy is effectively transmitted out of the domain. For the free-running model, the baroclinic southern boundary conditions are clamped to the BRAN3 boundary conditions to ensure accurate representation of the outflow to the south of the domain. Radiation conditions are applied to the east and west boundaries. For the assimilation, all three ocean boundaries are clamped in the baroclinic. Baroclinic energy that does not match the BRAN3 condition is absorbed at the boundaries using a flow relaxation scheme involving a sponge layer over which viscosity and diffusivity are increased linearly by a factor of 10 from the values applied within the model domain for the northern and eastern boundaries, and a factor of 20 for the southern boundary. The size of the sponge layer is 12 grid cells (approximately 60km). Because the BRAN3 system is run with different atmospheric forcing than we use, a correction was applied to the surface heat flux forcing such that the SST from BRAN3 is in balance with the atmospheric surface forcing for each month.

We begin by configuring a 10-year free-running simulation (hereafter referred to as the ‘10yr free run’) to ensure that the model is capable of representing the mean ocean circulation and its variability. The 10yr free run is also used to provide estimates of background variability to compute background error covariances for the assimilation scheme, and the 10-year mean Sea Surface Height (SSH) field is used for addition of Sea Level Anomaly (SLA) observations for assimilation into the model. For the 10yr free run we use atmospheric forcing from the National Center for Environmental Prediction’s (NCEP) reanalysis atmospheric model (Kistler et al., 2001). The atmospheric forcing fields are specified every 6 hours and used to compute the surface wind stress and surface net heat and freshwater fluxes using the bulk flux parameterisation of Fairall et al. (1996). A higher resolution atmospheric product was available for the 2-year reanalysis period. Atmospheric forcing for the 2-year model used to develop the reanalysis is provided by the 12km resolution Bureau of Meteorology (BOM) Australian Community Climate and Earth-System Simulation (ACCESS) analysis (Puri et al., 2013) and the forcing fields are specified every 6 hours.

## 2.2 Consistency of Free-running Model

The 10yr free run is performed from 2002–2011 as this is the most recent period over which BRAN3 data were available at the time of model development for use as initial and boundary forcing (BRAN3 more recently became available for the reanalysis period, 2012-2013). Comparison of the 10yr free run with observations provides validation of the ability of the model to represent the ocean dynamics in the region. The model reproduces well the spatial patterns of time-mean and variability of the mesoscale SSH; however, it is not expected to be in phase with the observations (e.g., the time and location of mesoscale eddies do not match). Figure 2 shows that the mesoscale SSH variability is well represented in the model compared to satellite-derived SSH data from AVISO over the 10-year period. This region of elevated SSH variability is consistent with the regions of enhanced eddy amplitude and rotational speed shown in Everett et al. (2012).

Mean cross-shore sections of alongshore velocity and temperature for the 10-year modelled period reveal a southward flowing EAC and the associated downward tilt of the thermocline (Figure 3). The sections shown cross the coast at the EAC Transport array, where the EAC is found to be most coherent (27.5° S), Coffs Harbour, just upstream of the typical EAC



separation zone ( $30.3^{\circ}$  S) and Sydney, downstream of the EAC separation zone ( $33.9^{\circ}$  S). The mean temperature sections compare well with the corresponding mean temperature sections from the CSIRO Atlas of Regional Seas (CARS) climatology (Ridgway et al., 2002).

Alongshore transport through the same three cross-shore sections for the full water column is computed daily and the mean, standard deviation, minimum and maximum transports are shown in Table 1. Mean transport at Coffs Harbour is greater than upstream at  $27.5^{\circ}$  S due to recirculation, as described by (Ridgway and Hill, 2009). The EAC typically separates from the coast south of Coffs Harbour and mean transport through the Sydney cross section is approximately one third of the transport at Coffs Harbour. This is consistent with Ridgway and Godfrey (1997), who estimate that about a third of the current's transport continues southward of the separation zone. Mata et al. (2000) compute transport from a mooring array located at  $30^{\circ}$  S, from the coast out the  $154.4^{\circ}$  E (a similar section to our Coffs Harbour section) between September 1991 and March 1994. They find a mean total transport of 22.1 Sv southward with an Root Mean Squared (RMS) variability of 30 Sv. This compares well with the transport through the Coffs Harbour section from the 10yr free run, which has a mean of 21.9 Sv poleward and a standard deviation of 31.7 Sv.

The model configuration is capable of producing the mean dynamical features of the EAC and representing the SSH variability. We aim to constrain the model with two years of observational data to examine the evolution of the EAC during this period.

### 3 Reanalysis Development

#### 3.1 Configuration

The reanalysis is configured for the 2-year period of 2012–2013 because of the availability of significant observational resources during this time; in particular, an ADCP and mooring array deployed to capture the transport of the EAC (as detailed in the next section). The reanalysis model uses atmospheric forcing provided by the 12km resolution BOM ACCESS analysis, which was not available to over the 10yr free run testing period described above. To ensure that the higher-resolution atmospheric forcing did not significantly alter the previous model comparison, we integrated the model for two years without assimilation (hereafter referred to as the '2yr free run') and compared the model-derived sea surface temperatures (SST) with those from the advanced very-high resolution radiometer (AVHRR) satellite data. The model and SST observations exhibit no net bias over the 2yr free run period (not shown). In addition, the vertical stratification of temperature and salinity of the 2yr free run well matches observations from Argo over that period (Figure 4).

#### 3.2 Data Assimilation Scheme

To generate the full reanalysis, we must combine this model with the observations in a way that uses the model physics to constrain the increments in initial conditions, boundary and surface forcing to generate a state estimate that better fits the observations. In this regard, we are looking for the model to represent the observations, not replicate the observations. If the



model is capable of representing all of the observations in time and space using the physics of the model, then we should have the most complete description of the ocean-state available. To accomplish this, we use incremental strong-constraint four-dimensional variational assimilation (IS4D-Var).

IS4D-Var is an advanced state estimation technique used to reduce the residuals between model output and observations in a way that is constrained by the dynamics of the flow. IS4D-Var uses variational calculus techniques to solve for the increments in model initial conditions, boundary conditions and forcing such that the difference between the modelled solution and all available observations is minimised – in a least-squares sense – over the assimilation window. The forward integration of the nonlinear model equations, given a prior estimate of the initial conditions, boundary and surface forcings, provides an estimate of the background state (the model prior). For each assimilation window we can formulate a cost function,  $J$ , that measures normalised deviations from the observations as well as from the model prior. The cost function is a function of the increment adjustment to the initial conditions, boundary conditions and forcing and has two terms. The first term represents the difference between the model and the observations, and is given by the squared difference between the observations and the model given the integration of the increment adjustment through the tangent linear model, weighted by the inverse of the observation error covariance. The second term penalises deviations from the background state, and is given by the squared difference between the new estimate and the background state, weighted by the inverse of the background error covariance.

The model prior is generated in the *outer* loop of the assimilation methodology. In order to improve the state estimate, the model initial conditions, boundary conditions and forcing are adjusted such that the quadratic cost function is minimised. The minimum is found by integrations of the tangent linear and adjoint models in the *inner* loops to determine the shape of the cost function, and the minimum is found where the gradient of the cost function goes to zero. The *inner* loops can be continued until  $J$  is reduced by a certain ratio, or, as in this study, a set number of *inner* loops can be completed that are found to give an acceptable reduction in  $J$ . We do not find the true minimum of  $J$ , but rather an acceptable reduction.

After the final *inner* loop the new increment is applied and the *outer* loop is completed by integrating the nonlinear model. The final *outer* loop provides the ‘best estimate’ of the ocean state (the analysis). The analysis is constrained to satisfy the nonlinear model equations (strong-constraint) and better represent the observations over the assimilation window, the length of which is limited by the time over which the tangent linear assumption remains reasonable. The analysis then provides an improved estimate of the initial state for the subsequent simulation window.

In any assimilation scheme, the prescribed prior uncertainties have a significant control on the assimilation procedure. The observation error covariance matrix specifies the uncertainty in the observations and the model’s ability to represent those observations so as to prevent “over-fitting” the solution to noisy observations. Defining these observational uncertainties is an important part of configuring any specific data assimilative model. Similarly, the background error covariance represents the uncertainty in our initial conditions, atmospheric forcing, and boundary conditions such that larger adjustments are permitted in regions where the uncertainties are high, and vice versa. The goal is to solve for the nonlinear ocean solution that is dynamically consistent with the observations and is free within the known uncertainties in the system. The resulting circulation has both a reduced uncertainty and better represents the observations.



Moore et al. (2011d) provide a detailed account of the IS4D-Var methodology and its mathematical formulation. The ROMS 4D-Var implementation is well described by (Moore et al., 2011d, b, c), and it has been used successfully in ROMS applications (e.g., Di Lorenzo et al. (2007); Powell et al. (2008); Powell and Moore (2008); Broquet et al. (2009); Matthews et al. (2012); Zavala-Garay et al. (2012); Janeković et al. (2013); Souza et al. (2014)).

### 5 3.3 Assimilation Configuration

The minimisation of the cost function,  $J$ , is performed in a sequence of linear least-squares minimisations in the *inner* loops, and the nonlinear model trajectory is updated in the *outer* loops. Because we are using 4D-Var, we aim for the longest time-window available without nonlinearities growing too large. Linearity experiments (not shown) found that for this region, the linear assumption remains acceptable for typical perturbations over 5 days, so we chose that as our window-size. Through experimentation, we found that one outer-loop, each with 14 inner-loops, gives an acceptable reduction in  $J$  for a feasible computational cost.

The ROMS 4D-Var allows for controlling both the initial conditions and the time-varying atmospheric and boundary forcing. We adjust the atmospheric forcing every 3 hours and the open boundary conditions every 12 hours. The winds are the dominant adjustment in the atmospheric forcing.

In this study, we use 5-day assimilation windows, with a one-day overlap. We overlap the assimilation windows by one-day, such that the initial conditions for the subsequent assimilation window are 4 days after the start of each window. The overlap allows us to produce a blended product by smoothing across the discontinuities between adjacent assimilation windows.

### 3.4 Observations and Observation Prior Uncertainties

The reanalysis time period was chosen because it contains the greatest number of available observations, including an EAC transport array that was deployed from 1 Apr 2012 to 26 Aug 2013. Other available subsurface observations and satellite-derived surface observations are also sourced for this time period. Figure 5a shows the Argo profiling float observations, coloured by time of occurrence, and Figure 5b shows all other observations, with the exception of the satellite-derived SSH, SST and Sea Surface Salinity (SSS). The number of processed observations assimilated for each 5-day assimilation window is shown in Figure 6a, with a break-down of the provenance of the temperature observations in Figure 6b. The observations and their respective processing for assimilation into the reanalysis are detailed in the subsections below.

The observations used for assimilation are limited by the spatial and temporal resolution of the model and the processes resolved. If multiple observations from the same instrument exist in the same horizontal and vertical grid cell taken within the same model time-step (5 minutes), the observations are averaged and this value is assimilated within that grid cell at the appropriate time. Representational errors are assigned to each observation and provide the uncertainty in the observation. This uncertainty is a combination of the uncertainty in the observation itself and just as significantly, the uncertainty in the model's ability to represent that observation. Observations of processes unresolved by the model must be either filtered or an uncertainty applied that accounts for the unresolved process. In the case of multiple observations in a single model grid cell, the variance of those observations provides a lower-bound to the representational error as the model can express only a single



value. Oftentimes, this error is greatest where the model resolution (and therefore its physics) cannot represent finer-scale dynamics captured in the observations.

We describe the observations used below and detail the observation uncertainties for each. The consistency of these estimates is checked with the posterior observation error in the results section.

### 5 3.4.1 Satellite-derived Sea Surface Height

Archiving, Validation and Interpretation of Satellite Oceanographic Data (AVISO), France, produce global, daily, gridded ( $1/4^\circ \times 1/4^\circ$ ) mean sea level anomaly (SLA) data produced by merging of all available satellites, computed with respect to a seven-year mean. The AVISO data provides a daily statistical field giving a synoptic view of the SSH. The AVISO SLA data is added to the dynamic SSH mean from the 10yr free run described above to generate sea level data for assimilation that is consistent with the ROMS model bathymetry and configuration.

We prescribe an observation uncertainty of 6cm. The error in the AVISO delayed-time global SLA product due to noise for the region is estimated at 2cm (CNES, 2015). We include a further 4cm of uncertainty because, in this case, the model resolves far more structure in the submesoscale than is capable in the observations. The AVISO fields provide a statistical fit to alongtrack SSH data and the observation uncertainty allows for imbalances between this statistical field and a dynamically balanced SSH field required by the model.

We exclude SSH observations that were taken over water depths less than 1000m. This is because the observations are noisy on the continental shelf and the AVISO gridded product is not able to resolve the submesoscale processes that occur here.

### 3.4.2 Satellite-derived Sea Surface Temperature

We use SST from the US Naval Oceanographic Office's Global Area Coverage Advanced Very High Resolution Radiometer level-2 product (NAVOCEANO's GAC AVHRR L2P SST). The product does not provide observations through clouds but contains useful observations close to the coast. Data is available 2-3 times per day. A product error is specified in the NAVOOCEANO SST product (Andreu-Burillo et al., 2010), with an error for each data point of  $0.38\text{-}0.4^\circ\text{C}$ . As the resolution of the data is similar to the resolution of the model, the observation uncertainty for the assimilation is set to the square of this product error.

### 25 3.4.3 Satellite-derived Sea Surface Salinity

Sea Surface Salinity (SSS) has been observed from space for the first time by the National Aeronautics and Space Administration's (NASA) Aquarius satellite ([www.aquarius.umaine.edu/](http://www.aquarius.umaine.edu/)). We make use of the Level 3 gridded salinity product which provides daily fields at a 1 degree resolution. The observation uncertainty is set to 0.4. There is a product error of around 0.2 for the Aquarius SSS data and 0.4 is chosen to account for additional uncertainty due to processes not resolved by the model. The value is considerably higher than the uncertainties specified for other *in-situ* salinity observations, so as to prevent the surface



salinity observations from dominating the salinity cost function. Similarly to SSH, any data taken over water depths less than 1000m depth were eliminated.

#### 3.4.4 Argo floats

Argo is an international program consisting of nearly 4,000 free-drifting profiling floats that measure the temperature and salinity of the upper 2000m of the global ocean ([www.argo.ucsd.edu](http://www.argo.ucsd.edu)). The Argo float locations in our model domain for 2011-2012, and the times at which they occur at those locations, are shown in Figure 5a. The Argo data points are averaged to the model grid and 5-minute time-step.

Uncertainty profiles are defined to specify the nominal minimal uncertainties for subsurface temperature and salinity. To devise the profile shapes, temperature and salinity variance is computed for each month of the year from the 10-yr free run. The monthly variances are spatially averaged over the model domain and averaged in time to give a single variance profile for both temperature and salinity. The profiles are then scaled to provide variance profiles appropriate for the nominal minimum observation error covariance. The uncertainty profiles are shown in Figure 7 (standard deviation is plotted instead of variance so the units are more intuitive for the reader). The profiles provide greater uncertainties in the depth ranges of greatest variability where representational errors are likely to be the largest. The representational error is specified as the maximum of this nominal minimum uncertainty and the variance of the observations from the same model cell. The uncertainties for Argo range from 0.12-1.2° C (0.06-0.16) for temperature (salt).

#### 3.4.5 Expendable Bathythermographs

Expendable Bathythermographs (XBT) collect temperature profiles along repeat lines sampled by merchant ships. Two transects intersect our model domain; PX34 which is the Sydney-Wellington route, and PX30 which is the Brisbane-Fiji route (only a small portion of this transect is within our model domain). Five PX30 lines took place over the assimilation period (16 Dec 2011, 8-9 Mar 2012, 13 Sep 2012, 7 Jun 2013 and 1 Nov 2013) and seven PX34 lines (3-4 Feb 2012, 23-24 May 2012, 22-23 Sep 2012, 26-27 Nov 2012, 16-18 Feb 2013, 12-13 May 2013 and 24-26 Aug 2013). The sections are sampled at 10km intervals. The XBT data points are averaged to the model grid and 5-minute time-step.

The same nominal minimal uncertainty profile used for the Argo temperature observations (Figure 7) is used.

#### 3.4.6 High-Frequency Radar

The Coffs Harbour High-Frequency (HF) ocean radar is part of the IMOS and is managed by the Australian Coastal Ocean Radar Network (ACORN, <http://imos.org.au/acorn.html>). The radar is a WERA phased array system with 16-element receive arrays located at Red Rock to the north of Coffs Harbour (RRK, 29.98° S , 153.23° E) and North Nambucca to the south (NNB, 30.62° S , 153.011° E). The radars operate at a frequency of 13.920 MHz, with a bandwidth of 100 KHz and a maximum range of 100 Km.



The HF radar broadcasts and receives along defined angles in a phased-array setup and the surface current speed (towards and away from the radar site) is measured. The overlapping coverage from the two radar sites allows the surface current ( $u$  and  $v$ ) vectors to be computed. Using the same assimilation procedure as detailed in Souza et al. (2014), we assimilate radial currents, rather than the computed current velocities. The velocities have correlated errors and using the radials allows us to make use of data when only one station is available and over areas that do not overlap with the other station's measurements. We can also make use of radial data in regions where the beam intersection angle between measurements from the two stations results in high error in the velocity calculation while the radials errors are adequately low.

Radial data is available from 1 Mar 2012 to the end of the reanalysis period. The areas of HF radar coverage are shown in Figure 5b, with inset panels showing the percentage of data coverage for assimilated radials for the RRK and NNB sites in Figure 5c and 5d, respectively. Radials for each of the two stations are processed separately. At the outer range of the HF radar instrument coverage, radial values become noisy. We extract only radial values with Bragg Signal to Noise ratio  $>10$  dB. Manual inspection of the radial values for each of the two sites was then conducted and a “good data” region was chosen for each site every day, excluding the outer regions of coverage where noisy data is observed. Only radial data within these “good data” regions is used, and absolute radial speed values greater than  $2 \text{ ms}^{-1}$  are excluded. This manual inspection was performed daily as the radii of reliable radial data varies significantly, and this method allows us to retain the maximum amount of data for assimilation. The radial speeds and angles are spatially averaged onto the model grid and a 24-hour boxcar averaging filter is used to remove tides and inertial oscillations that are not resolved by the model.

Radial speed standard error is given in the data files provided by ACORN, calculated from the mean width of the two Bragg peaks weighted by their maximum power (Wyatt, 2014). These standard errors are converted to variances and averaged as above. An error variance is then applied to each observation, given by the maximum of the averaged variances and the variance of the averaged radial speeds. The nominal minimum observation error for the surface radials is set to  $0.15 \text{ ms}^{-1}$ . The observation error covariance for each radial speed observation is set to the maximum of the nominal minimum observation error covariance and the error variance computed during the averaging.

Any observations where the square-root of the radial speed error variance exceeds the radial speed magnitude are removed. Radial data within one grid cell of the coast is also removed as unrealistically high values are observed here.

### 3.4.7 NSW Shelf Moorings

Data collected from 3 moorings located along the NSW continental shelf is used in this assimilation study. The moorings collect temperature and velocity data at high sampling frequencies and are located off of Coffs Harbour,  $30^\circ \text{ S}$  (CH100) and Sydney,  $33.9^\circ \text{ S}$  (SYD100 and SYD140). In each case the number in the mooring name represents the approximate water depth of the mooring location. Table 2 contains details of the mooring locations and the properties observed. Temperature sensors are spaced every 8 meters. The data collection and quality control is described in detail in Roughan and Morris (2011).

All temperature observations taken from moorings at high sampling frequencies are low-pass filtered to remove variability at periods shorter than the inertial period (23.8 hours for Coffs Harbour and 21.5 hours for Sydney), and the observations are applied 6-hourly. For latitudes south of  $30^\circ \text{ S}$ , the inertial period is less than 24 hours so the filtering does not remove the diurnal



signal which may arise from internal tides and/or diurnal surface heating for near surface temperature observations. The RMS residual between the mooring temperature observations low-pass filtered at 30 hours (removing variability due to baroclinic tides and inertial oscillations) and the observations filtered at the inertial frequency is very small compared to the nominal minimum uncertainties applied, confirming that these unresolved processes are accounted for in the observation uncertainty specification. Velocity observations are low-pass filtered at 30 hours to remove variability due to tides and inertial oscillations and applied 6-hourly. It is important to remove the tidal signal from velocity observations as the barotropic tidal velocities are of similar order of magnitude to the sub-tidal velocities.

For all observations on the continental shelf, different nominal minimum observation uncertainty profiles are adopted (to those used offshore for Argo and XBT) to account for increased variability due to finer scale processes that occur on the shelf that are not resolved in the model. Variance profiles for the shelf observations were computed by comparing all of the shelf observations (NSW moorings, SEQ moorings and gliders) to the 2yr free run for the 2012-2013 assimilation period to generate a nominal uncertainty profile on the shelf. Profiles were generated for all observed *in situ* variables; *u* and *v* velocity components, temperature, and salinity. *u* (*v*) uncertainty peaks at 0.12 (0.3)  $\text{ms}^{-1}$  in the upper 50m reducing to 0.08 (0.1)  $\text{ms}^{-1}$  at 200m depth. The shelf temperature uncertainty profile peaks at 1.2° C between 20-100m depth, reducing to 0.8° C at 200m. The computed salinity errors were doubled and are 0.1-0.16 for the upper 200m on the shelf.

The observation error is specified as the maximum of this nominal minimum error and the variance from averaging observations within the same model grid cell. For velocities, the high density of the ADCP depth bins means several velocity measurements are often available for a single vertical grid layer, which can result in variances that exceed the specified nominal minimum uncertainty.

#### 3.4.8 EAC Transport Array and SEQ Shelf Moorings

The EAC transport array was deployed as part of the IMOS to understand the variability of the EAC, and it is comprised of five deep water moorings (EAC 1-5) which measure temperature, salinity and velocities. The array was positioned where the EAC is predicted to be most coherent and was designed to measure the mean and time-varying EAC transport (Sloyan et al., 2016). The array is continued onto the shelf slope and shelf with two moorings (SEQ400 and SEQ200) in approximate water depths of 400m and 200m, respectively. Each mooring has a suite of instruments measuring temperature, salinity, and velocities at high sampling frequencies throughout the water column. Table 2 contains details of the moorings.

All temperature and salinity observations are low-pass filtered to remove variability at periods shorter than the inertial period (26.0 hours), and the observations are applied 6-hourly. The vertical uncertainty profile used for the other off-shelf temperature and salinity observations (Figure 7) is used for the nominal minimum profile for the EAC array mooring observations. For the SEQ moorings the nominal minimum vertical uncertainty profile generated for the shelf observations was used. The velocity observations are filtered and processed in the same manner as the NSW moorings, described above. For the EAC array moorings, the nominal minimum error for *u* and *v* velocity components was specified as 0.12  $\text{ms}^{-1}$  in the upper 10m of the water column and 0.10  $\text{ms}^{-1}$  for all depths below 10m. For the SEQ moorings, the uncertainty profile generated for the



shelf observations was used. Similarly to the NSW moorings, the observation uncertainty is specified as the maximum of this nominal minimum uncertainty and the variance from averaging observations within the same model grid cell.

### 3.4.9 Ocean Gliders

Autonomous ocean gliders (both SeaGliders and Slocum) were deployed as part of the IMOS by the Australian National Facility for Ocean Gliders (<http://imos.org.au/anfog.html>). The buoyancy controlled gliders move horizontally through the water while collecting vertical profiles of temperature and salinity. The majority of the glider missions in the model domain over the 2011–2012 time period occur on the NSW continental shelf, between 29.5° S and 32.3° S, with two missions between 25 March 2013 and 22 July 2013 extending offshore, further south and to depths of 900m (Figure 5b). Quality control flags are applied to the glider data through the IMOS processing (Australian National Facility for Ocean Gliders, 2012) and only the data deemed to be “top quality data in which no malfunctions have been identified and all real features have been verified during the quality control process” are used. The glider data points are averaged onto the model grid and 5-minute time-step.

Glider temperature data in the upper 20m and salinity data in the upper 50m were removed. The uncertainty profiles computed for the shelf observations were used and the uncertainties for the gliders are the maximum between the variance computed from the averaging and the shelf uncertainty profile.

### 3.5 Model Prior Uncertainties

The goal of the assimilation is combine an uncertain model with uncertain observations to reduce the analysis uncertainty to be lower than the model prior. As such, specification of the prior model and observation uncertainties is important. The model uncertainty should represent the uncertainty in the state of the model for the given time. This was estimated from the average of 5-day variances from the 10yr free run described above. The variances provide an estimate of the uncertainty associated with each state variable and surface forcing field. We choose 5-day variances as the model is nested in BRAN3 which assimilates large-scale data so we expect our model prior boundary and initial conditions to be accurate to within the typical changes to the ocean state that occur over 5-days. Because we have only estimates of the variances, the background error covariance of each field is estimated via a diffusion operator with specified length-scales that are assumed to be homogeneous and isotropic.

In the horizontal, the characteristic length scales chosen for the background covariance are 100km for SSH, temperature and salinity and 70km for velocities. These values were chosen based on analysis of cross-correlation of SSH and complex correlation of surface velocities between points in the eddy rich Tasman Sea region from the 2yr free run. The length scale of 100km for SSH is consistent with the decorrelation scales estimated from along-track satellite data for the area by Wilkin et al. (2002) and used by Zavala-Garay et al. (2012). It is noted that shorter cross-shore length scales are likely along the coast of south-eastern Australia, as the continental shelf is narrow (15-30km) and the EAC displays a narrow jet like structure, while SSH decorrelation length scales were found to be about 100-200km in the alongshore direction by Oke and Sakov (2012). Bridging the scales between mesoscale eddy variability in the Tasman Sea and smaller-scale shelf processes, and the anisotropic flow regime, is a challenge and the impact of the horizontal length scale specification requires further research.



For the vertical, semivariogram analysis of glider data on the NSW shelf by Schaeffer et al. (2015) found vertical decorrelation length scales of about 50m for both temperature and salinity on the NSW shelf. Analysis of correlations between temperature data measured by the moorings used in this study found vertical decorrelation length scales of 15-30m for the shelf moorings (NSW moorings, SEQ 200), 70m for SEQ 400 and 100-200m for the EAC deepwater array moorings (EAC 1-5). Salinity measurements were taken at SEQ200, SEQ400 and the EAC deep water array moorings and decorrelation length scales were similar to the length scales for temperature at these moorings. In the vertical, we apply characteristic length scales of 50m for salinity and 10m for temperature. The shorter length scale for temperature was adopted due to the short length scale of variability for temperature near the sea surface, as SST observations dominate. The salinity length scale is set to 50m (longer than the temperature length scale) in order to limit vertical structure in the salinity analysis increments.

Analysis of correlations between velocities measured by the moorings found vertical decorrelation length scales of 20-50m for the shelf moorings (NSW moorings, SEQ 200), 70m for SEQ 400 and 100-200m for the the EAC deep water array moorings (EAC 1-5). Because the deep water moorings span the core of the EAC, we reduced the decorrelation length scale value to 50m in the vertical for velocity to be ensure consistency when assimilating velocities outside of the EAC and/or on the shelf.

The covariances (between differing model variables) are computed by the tangent linear and adjoint models in the *inner* loops. The uncertainty in the observations are detailed below.

## 4 Reanalysis Evaluation

In this section, we evaluate the performance of the assimilation procedure in terms of the consistency between the posterior and prior uncertainties, comparison with the observations, and comparison to unassimilated observations. Overall, the assimilation performs well in minimising the cost function over each assimilation interval and the corresponding reanalysis provides a good match to observations.

### 4.1 Consistency of Observation and Model Uncertainties

The level of agreement between the prior observation and model uncertainty specified and the posterior uncertainty from the assimilation provides a measure of the consistency of the assimilation system given the prior uncertainty assumptions (Desroziers et al., 2005). The posterior errors are calculated for the reanalysis using equations (5) and (6) in Moore et al. (2011a). The calculations are in observation space and the prior and posterior uncertainties match well.

For SSH, the spatially-averaged posterior observation uncertainty ranges from 4.1-8.6cm with a mean value of 5.7cm, which matches the prior observation uncertainty of 6cm very well. The SSH prior and posterior model uncertainties are also consistent. For subsurface temperature, the prior and posterior model uncertainties match very well. The prior observation uncertainties are greater than the posterior observation uncertainties for subsurface temperature; the time-mean of the spatially-averaged prior uncertainties is  $0.88^{\circ}$  C compared to  $0.50^{\circ}$  C for the posterior uncertainties. This prior uncertainty was necessary to account for the errors of representativeness associated with the subsurface temperature observations. Similarly for subsurface salinity and velocities, the prior observation uncertainties exceed the posterior observation uncertainties. For the radial velocities, the



time-mean of the spatially-averaged posterior observation uncertainties is  $0.12\text{ms}^{-1}$ , which matches the prior observation uncertainty of  $0.15\text{ms}^{-1}$  well.

Overall, we are confident that the prior uncertainties are well specified and, as such, the assimilation is configured to provide a near-optimum minimisation of the cost function for each assimilation interval.

## 5 4.2 Reanalysis Comparison to Observations

### 4.2.1 SSH

The Root Mean Squared (RMS) observation anomaly for a particular observation location describes the variability in the observation with respect to its time-mean. This is compared to the RMS differences between the observations and the free-running model (the 2yr free run), and the observations and the analysis, to provide an assessment of how well the free run and the analysis match the observations relative to their typical variability. A skillful state estimate will have residuals with the observations that are much lower than the observation's typical variability.

The observation anomaly for an observed variable  $v$  at a particular location is given by  $RMS_{ObsAnom} = \sqrt{\frac{\sum_{t_1}^{t_n} (v(t) - \bar{v})^2}{n}}$ , where  $t = t_1 - t_n$  are the observation times and  $\bar{v}$  is the time-mean of the observed variable at that location. The RMS difference between the free run values (in observation space) and the observations and the analysis and observations are given by  $RMSD_{Freerun-Obs} = \sqrt{\frac{\sum_{t_1}^{t_n} (v_f(t) - v_o(t))^2}{n}}$  and  $RMSD_{Analysis-Obs} = \sqrt{\frac{\sum_{t_1}^{t_n} (v_a(t) - v_o(t))^2}{n}}$ , respectively, where  $v_o$  is the observed value,  $v_f$  is the corresponding value from the free run and  $v_a$  is the corresponding value from the analysis.

Figure 8a shows the RMS SSH anomaly from the observations over the 2-year assimilation period. The  $RMSD_{Analysis-Obs}$  is shown in Figure 8b and shows that the SSH fields are well represented in the analyses. In Figure 8c, the domain-averaged  $RMS_{ObsAnom}$ ,  $RMSD_{Freerun-Obs}$  and  $RMSD_{Analysis-Obs}$  are plotted for each 5-day assimilation window over the 2-year period, showing significant improvement in the fit to observations in the analyses. The  $RMSD_{Freerun-Obs}$  is of similar magnitude to the SSH observation anomaly indicating that, as expected, the free run has no skill in predicting the chaotic mesoscale eddies. The time-mean of the spatially-averaged  $RMSD_{Analysis-Obs}$  over all assimilation windows is 7.4cm. This is close to the observation uncertainty for SSH of 6cm and small compared to the typical SSH variability (the time-mean of the spatially-averaged SSH observation anomalies is 23.4cm)

### 25 4.2.2 SST

The free-running model shows some skill in prediction of the SST due to the accuracy of the surface forcing; however, significant improvement is achieved in the analyses. The RMS SST observation anomalies describe the variability in SST over the 2-year assimilation period, including the seasonal cycle, and are shown in Figure 9a. The  $RMSD_{Freerun-Obs}$  is smaller than the observation anomalies and the  $RMSD_{Analysis-Obs}$  (Figure 9b) is further reduced. The time-series of spatially-averaged  $RMS_{ObsAnom}$ ,  $RMSD_{Freerun-Obs}$  and  $RMSD_{Analysis-Obs}$  are shown in Figure 9c over the 2-year period. The time-mean of the spatially-averaged analysis error for all assimilation windows is  $0.4^\circ\text{C}$ , which is the same magnitude as the SST observa-



tion uncertainty. The high variability seen in the time-series plots, particularly in the observation anomaly, is due to the patchy spatial coverage of the SST observations.

### 4.2.3 Subsurface temperature from Argo, Gliders and XBT

Subsurface observations are spatially and/or temporally sparse in comparison to satellite observations of the sea surface. The covariances between surface and subsurface variables are computed with the adjoint and tangent-linear model such that the model physics are used to generate the time-varying covariance. While these covariances allow the surface observations to impact state estimates of the subsurface properties, subsurface observations are invaluable in improving estimates of the subsurface (e.g., Zavala-Garay et al. (2012)).

We show the improvement in subsurface temperature as measured by the Argo floats, XBTs and ocean gliders by computing the  $RMSD_{FreeRun-Obs}$  and  $RMSD_{Analysis-Obs}$  in nominal depth bins for all observations over the model domain (Figure 10). For Argo, time-mean  $RMSD_{FreeRun-Obs}$  for all observations in the upper 500m of the water column is  $1.6^{\circ}\text{C}$ , reduced to  $0.8^{\circ}\text{C}$  in the analysis. For the XBT above 500m, the time-mean RMSD is reduced to  $1.2^{\circ}\text{C}$  in the analysis from  $2.0^{\circ}\text{C}$  for the free-running model. Below 500m, the number of observations in each depth bin for Argo and XBT is too low for a meaningful comparison. The greatest improvement in the fit to observations is achieved in the glider data which mostly samples the shelf and shelf slope circulation. A great majority of the glider observations are in the upper 100m of the water column; here the time-mean  $RMSD_{FreeRun-Obs}$  of  $1.9^{\circ}\text{C}$  is reduced to  $0.9^{\circ}\text{C}$  in the analysis.

As the Argo profiling floats measure both temperature and salinity at each observation time we are able to assess the residual reduction in terms of potential density throughout the water column (Figure 11), describing the improvement in the representation of the density structure in the analysis. The free-running model has some skill in predicting potential density as sampled by the Argo floats in the upper 500m, as the  $RMSD_{FreeRun-Obs}$  is less than the  $RMS_{ObsAnom}$  for the nominal depth bins. The  $RMSD_{Analysis-Obs}$  in potential density is reduced to about half of the  $RMSD_{FreeRun-Obs}$  in the upper 500m; the upper layer that is most effected by mesoscale eddies. The  $RMSD_{Analysis-Obs}$  in potential density peaks in the upper 100m at  $0.24\text{kgm}^{-3}$  and decreases gradually to below  $0.1\text{kgm}^{-3}$  at 500m depth, remaining below that for the Argo-observed ocean deeper than 500m.

### 4.2.4 Mooring observations

Profiles of the complex correlation between the velocities from the free-running model and the analyses at the mooring velocity measurement locations are shown in Figure 12. The correlations are generally considerably improved in the analyses. The complex correlations for the analysis velocities approach the value of one for the South East Queensland shelf moorings (SEQ200 and SEQ400), which are on the shelf and shelf slope at the latitude where the EAC is found to be most coherent. At this same latitude, the deep water array moorings 1 to 4 (EAC1-4) have high complex correlations between the analysis and the observations in the upper 400m of the water column. This is where the mean EAC jet is the strongest (refer to Figure 3). The EAC5 mooring is outside of the main jet and influenced by a more variable eddy-dominated circulation and the analysis has slightly lower correlations in the upper water column at this location.



Further south on the shelf, velocity estimates are improved with depth-averaged free run and analysis complex correlations of 0.69 and 0.91, respectively, for the Coffs Harbour mooring (CH100), 0.50 and 0.83 for the Sydney mooring (SYD100) and 0.48 and 0.87 for the other Sydney mooring (SYD140).

#### 4.2.5 Radials

5 The observed surface velocities are computed from the assimilated radials and the corresponding values computed from the radial values extracted from the free-running model and the analyses. The complex correlations between these observed surface velocities and the surface velocities computed from the free-running model and the analysis are shown in Figure 13. Note that the complex correlation for a particular grid cell requires velocities to be computed, which requires radial data from each of the two sites to be available in that cell and that the beams overlap with an angle greater than  $30^\circ$  (velocity calculations where  
 10 beam intersection angles are smaller than this are deemed inaccurate). Radial data is assimilated at other times but cannot be converted to velocities. Only grid cells where velocity values can be computed at more than 10 times over the 2-year period are included in the plots. Surface velocities are compared here (rather than the scalar radial velocity values) as they are more meaningful in terms of the ocean surface currents. In the free run, velocity estimates were best on the shelf and shelf slope with complex correlations reducing offshore of the shelf slope. Velocity is very well represented in the analysis under the HF radar  
 15 footprint, with complex correlations from 0.8-1 across the entire footprint.

#### 4.3 Comparison to independent observations

Because 4D-Var uses the model dynamics to determine covariance, information from observed variables can propagate to unobserved regions such that the ocean state better fits and is in balance with the observations. Comparison of the reanalysis with independent, non-assimilated, observations allows us to assess the performance of the state estimate away from assimilated  
 20 observations. As the principal aim of this work was to assimilate the maximum number of available observations in the region in order to provide a ‘best estimate’ of the ocean state over the 2-year period, few independent observations remain available for this comparison.

The available independent observations are from shipboard CTD casts that were taken on three separate cruises within the model domain over the 2-year period. 15 CTD casts were taken as part of the deployment of the EAC array, along the EAC  
 25 array transect from 21-27th April 2012. 5 casts were taken off of Sydney between  $34.3\text{--}36.4^\circ$  S and  $151.6\text{--}152.8^\circ$  E from 27-28 Feb 2013. 28 CTD casts were taken in two transects off of Brisbane at  $26.3^\circ$  S and  $27.1^\circ$  S out to  $155.8^\circ$  E between 21-31 Aug 2013. The CTD cast observations are mapped to the model vertical levels for consistent comparison given the vertical discretisation of the model, and the corresponding model values extracted from the 2yr free run and the analysis. The  $RMS_{ObsAnom}$ ,  $RMSD_{FreeRun-Obs}$  and  $RMSD_{Analysis-Obs}$  for potential density in nominal depth bins for all CTD casts are  
 30 shown in Figure 14a. In the upper 350m of the water column, the  $RMSD_{Analysis-Obs}$  in the potential density is reduced to about half of  $RMSD_{FreeRun-Obs}$ . For all CTD casts in the upper 200m, where the number of observations is the greatest (not shown), the depth-averaged  $RMSD_{FreeRun-Obs}$  of  $0.35 \text{ kgm}^{-3}$  is reduced to  $0.18 \text{ kgm}^{-3}$  in the analysis. This shows a marked improvement in the representation of the subsurface ocean, as observed by these CTD casts, is achieved in the reanalysis.



Note that the profiles of Argo  $\text{RMSD}_{\text{Freerun-Obs}}$  and  $\text{RMSD}_{\text{Analysis-Obs}}$  in potential density (Figure 11) are similar to the RMSD profiles for the independent shipboard CTD observations. The reanalysis showing similar residual reduction for the assimilated Argo observations and for the non-assimilated CTD cast observations suggests a well-specified assimilation system in which a dynamically-balanced ocean state estimate is achieved with improved state-estimation throughout the model domain, rather than over-fitting to assimilated observations.

## 5 Summary and Conclusions

We have presented the development of a data assimilating model of the EAC region and assessed the performance of the corresponding reanalysis over a 2-year period. We use an advanced variational data assimilation scheme to integrate a state-of-the-art coastal ocean model with an unprecedented observational data for the southeast Australian region. We show that the free-running numerical model reproduces the long-term mean surface and subsurface ocean properties and represents the eddying circulation as expressed by the sea surface variability well. For the reanalysis, we show that the SSH and SST have mean RMS residuals with the observations of 7cm and 0.4° C. The RMS residual profile for temperature has a subsurface maximum of 1° C for Argo float observations, 1.4° C for ocean glider observations and 1.7° C for XBT observations. Surface and subsurface velocity observations from HF radar, shelf and offshore moorings match well with complex correlations between 0.8-1 in the upper 500m. The reanalysis has an RMS residual in potential density with independent (non-assimilated) shipboard CTD cast observations of under 0.2  $\text{kgm}^{-3}$  throughout the water column.

The performance of the reanalysis is dependent on prior assumptions of the observation and model error covariances and we show that the prior and posterior observation and model uncertainties are consistent. This indicates that the assimilation configuration allows a near-optimum minimisation of the difference between the observations and the model, given observation and model uncertainty. This is achieved through processing of the observations to eliminate fine-scale processes not resolved by the model, and through careful specification of the prior observation and model background uncertainties.

Not only does the reanalysis provide a good match with observations, it is the first reanalysis of the EAC region that resolves the continental shelf at its narrowest point (15km) by more than a single grid cell (BRAN3 has a resolution of 10km, Oke et al. (2013)) and the first high-resolution reanalysis of the region that uses the model physics to adjust the model in a dynamically consistent way (Zavala-Garay et al. (2012) has a resolution of 18-30km). Furthermore, it is the first attempt to assimilate such a variety of observations in the region, including observations from moorings on and off the continental shelf, a coastal HF radar array and ocean gliders. The high-resolution and dynamic-consistency of the reanalysis mean it has the potential to provide a marked improvement in our ability to capture important circulation dynamics in the EAC.

The reanalysis is being used to study the 3-dimensional structure of the current and the processes that drive its separation from the coast and eddy formation. Several modelling studies of coastal regions in south-eastern Australia are making use of the reanalysis for boundary forcing. Output from the adjoint model integrations performed in each assimilation interval is being used to directly assess the impact of specific observations on the estimates of circulation dynamics of interest. Through this we hope to understand which observations are most effective at improving our state-estimates and which locations are most



effective to observe, providing valuable information on how we might improve the observing system to ultimately improve prediction.

## 6 Data availability

Model initial conditions and boundary forcing comes from the Bluelink ReANalysis version 3p5 (BRAN3, Oke et al. (2013)).

- 5 Surface forcing is provided by the Australia Bureau of Meteorology's Australian Community Climate and Earth-System Simulation (ACCESS) 12km product (Puri et al., 2013). The observations used for assimilation are available through the Australian Integrated Marine Observing System's (IMOS) data portal ([www.imos.org.au](http://www.imos.org.au)).

The reanalysis output is saved as snapshots of 3-dimensional fields of ocean properties (sea-level, temperature, salinity, velocities) every 4 hours over the 2-year period (2012-2013). The data is archived at the University of New South Wales,

- 10 Australia, and can be made available for research purposes (contact the corresponding author of this paper).

*Acknowledgements.* We thank Dr. Holly Sims from the BOM for making ACCESS available to us and Dr. Gary Brassington, also from the BOM, for providing data in the preliminary phases of this work and for his useful discussions. The XBT data was kindly provided by Ken Ridgeway of CSIRO Hobart.



## References

- Andreu-Burillo, I., Brassington, G., Oke, P., and Beggs, H.: Including a new data stream in the BLUElink Ocean Data Assimilation System, *Aust. Meteorol. Ocean.*, 59, 77–86, 2010.
- Australian National Facility for Ocean Gliders: Data Management, 2012.
- 5 Broquet, G., Edwards, C. A., Moore, A., Powell, B. S., Veneziani, M., and Doyle, J. D.: Application of 4D-Variational data assimilation to the California Current System, *Dynam. Atmos. Oceans*, 48, 69–92, 2009.
- Cetina Heredia, P., Roughan, M., Van Sebille, E., and Coleman, M.: Long-term trends in the East Australian Current separation latitude and eddy driven transport, *J. Geophys. Res.*, 119, 2014.
- Chapman, D. C.: Numerical treatment of Cross-Shelf Open Boundaries in a Barotropic Coastal Ocean Model, *J. Phys. Oceanogr.*, 15, 1060–  
10 1075, 1985.
- CNES: SSALTO/DUACS User Handbook: (M)SLA and (M)ADT Near-Real Time and Delayed Time Products, AVISO Satellite Altimetry Data, 2015.
- Desroziers, G., Berre, L., Chapnik, B., and Poli, P.: Diagnosis of observation, background and analysis-error statistics in observation space., *Quarterly Journal of the Royal Meteorological Society*, 131, 3385–3396, 2005.
- 15 Di Lorenzo, E., Moore, A. M., Arango, H. G., Cornuelle, B. D., Miller, A. J., Powell, B. S., Chua, B. S., and Bennett, A. F.: Weak and Strong Constraint Data Assimilation in the inverse Regional Ocean Modelling System (ROMS): development and application for a baroclinic coastal upwelling system, *Ocean Modelling*, 16, 160–187, 2007.
- Everett, J. D., Baird, M. E., Oke, P. R., and Suthers, I. M.: An avenue of eddies: Quantifying the biophysical properties of mesoscale eddies in the Tasman Sea, *Geophys. Res. Lett.*, 39, 2012.
- 20 Fairall, C. W., Bradley, E. F., Rogers, D. P., Edson, J. B., and Young, G. S.: Bulk parameterization of air-sea fluxes for tropical ocean-global atmosphere Coupled-Ocean Atmosphere Response Experiment, *J. Geophys. Res.*, 101, 3747–3764, 1996.
- Feron, R. C. V.: The southern ocean western boundary currents: Comparison of fine resolution Antarctic model results with Geosat altimeter data, *J. Geophys. Res.*, 100, 4959–4975, 1995.
- Ferrari, R. and Wunsch, C.: Ocean Circulation Kinetic Energy: Reservoirs, Sources, and Sinks, *Annu. Rev. Fluid Mech.*, 41, 253–282, 2009.
- 25 Flather, R. A.: A tidal model of the northwest European continental shelf, *Mem. Soc. R. Sci. Liege*, 6, 141–164, 1976.
- Gordon, A. L., Horai, K. I., and Donn, M.: Southern hemisphere western boundary current variability revealed by GEOS 3 altimeter, *J. Geophys. Res.*, 88, 755–762, 1983.
- Haidvogel, D. and Beckmann, A.: *Numerical Ocean Circulation Modeling*, Imperial College Press, 1999.
- Haidvogel, D. B., Arango, H. G., Hedstrom, K., Beckmann, A., Malanotte-Rizzoli, P., and Shchepetkin, A. F.: Model evaluation experiments  
30 in the North Atlantic Basin: simulations in nonlinear terrain-following coordinates, *Dynam. Atmos. Oceans*, 32, 239–281, 2000.
- Haney, R. L.: On the Pressure Gradient Force over Steep Topography in Sigma Coordinate Ocean Models, *J. Phys. Oceanogr.*, 21, 610–619, 1991.
- Janeković, I., Powell, B. S., Matthews, D., McManus, M. A., and Sevdjian, J.: 4D-Var Data Assimilation in a Nested, Coastal Ocean Model: A Hawaiian Case Study, *J. Geophys. Res.*, 118, 1–14, doi:10.1002/jgrc.20389, 2013.
- 35 Kistler, R., Kalnay, E., Collins, W., Saha, S., White, G., Woolen, J., Chelliah, M., Ebisuzaki, W., Kanamitsu, M., Kousky, V., van den Dool, H., Jenne, R., and Fiorino, M.: The NCEP/NCAR 50-Year Reanalysis, *Bull. Am. Met. Soc.*, 82, 247–268, 2001.



- Macdonald, H. S., Roughan, M., Baird, M. E., and Wilkin, J.: A numerical modeling study of the East Australian Current encircling and overwashing a warm-core eddy, *J. Geophys. Res.*, 118, 301–315, 2013.
- Macdonald, H. S., Roughan, M., Baird, M. E., and Wilkin, J.: The formation of a cold-core eddy in the East Australian Current, *Continental Shelf Research*, 2014.
- 5 Mata, M. M., Tomczak, M., Wijffels, S. E., and Church, J. A.: East Australian Current volume transports at 30°S: Estimates from the World Ocean Circulation Experiment hydrographic sections PR11/P6 and the PCM3 current meter array, *Journal of Geophysical Research*, 105, 28 509–28 526, 2000.
- Mata, M. M., Wijffels, S. E., Church, J. A., and Tomczak, M.: Eddy shedding and energy conversions in the East Australian Current, *Journal of Geophysical Research*, 111, 2006.
- 10 Matthews, D., Powell, B. S., and Janeković, I.: Analysis of Four-dimensional Variational State Estimation of the Hawaiian Waters, *J. Geophys. Res.*, 117, doi:10.1029/2011JC007575, 2012.
- Mellor, G. L. and Yamada, T.: Development of a turbulence closure model for geophysical fluid problems, *Rev. Geophys. Space Phys.*, 20, 851–875, 1982.
- Mellor, G. L., Ezer, T., and Oey, L. Y.: The pressure gradient error conundrum of sigma coordinate ocean models, *J. Atmos. Ocean. Technol.*, 15, 1126–1134, 1994.
- Moore, A., Arango, H. G., Di Lorenzo, E., Miller, A. J., and Cornuelle, B. D.: An Adjoint Sensitivity Analysis of the Southern California Current Circulation and Ecosystem, *J. Phys. Oceanogr.*, 39, 702–720, 2009.
- Moore, A. M., Arango, H. G., Broquet, G., Edwards, C., Veneziani, M., Powell, B., Foley, D., Doyle, J. D., Costa, D., and Robinson, P.: The Regional Ocean Modelling System (ROMS) 4-dimensional variational data assimilation systems: Part 11 - Performance and application to the California Current System, *Progress in Oceanography*, 91, 50–73, 2011a.
- 20 Moore, A. M., Arango, H. G., Broquet, G., Edwards, C., Veneziani, M., Powell, B. S., Foley, D., Doyle, J., Costa, D., and Robinson, P.: The Regional Ocean Modeling System (ROMS) 4-dimensional variational data assimilation systems: Part II – Performance and application to the California Current System, *Prog. Oceanog.*, 91, 50–73, doi:10.1016/j.pocean.2011.05.003, 2011b.
- Moore, A. M., Arango, H. G., Broquet, G., Edwards, C., Veneziani, M., Powell, B. S., Foley, D., Doyle, J., Costa, D., and Robinson, P.: The Regional Ocean Modeling System (ROMS) 4-dimensional variational data assimilation systems: Part III – Observation impact and observation sensitivity in the California Current System, *Prog. Oceanog.*, 91, 74–94, doi:10.1016/j.pocean.2011.05.005, 2011c.
- 25 Moore, A. M., Arango, H. G., Broquet, G., Powell, B. S., Zavala-Garay, J., and Weaver, A. T.: The Regional Ocean Modeling System (ROMS) 4-dimensional variational data assimilation systems: Part I – System overview and formulation, *Prog. Oceanog.*, 91, 34–49, doi:10.1016/j.pocean.2011.05.004, 2011d.
- 30 Oke, P., Sakov, P., Cahill, M. L., Dunn, J. R., Fiedler, R., Griffin, D. A., Mansbridge, J. V., Ridgway, K. R., and Schiller, A.: Towards a dynamically balanced eddy-resolving ocean reanalysis: BRAN3, *Ocean Modell.*, 67, 52–70, 2013.
- Oke, P. R. and Middleton, J. H.: Topographically Induced Upwelling off Eastern Australia, *Journal of Physical Oceanography*, 30, 512–530, 2000.
- Oke, P. R. and Sakov, P.: Assessing the footprint of a regional ocean observing system, *Journal of Marine Systems*, in press, 2012.
- 35 Oke, P. R., Schiller, A., Griffin, D. A., and Brassington, G. B.: Ensemble data assimilation for an eddy-resolving ocean model of the Australian region, *Q. J. R. Meteorol. Soc.*, 131, 3301–3311, 2005.
- Oke, P. R., Brassington, G. B., Griffin, D. A., and Schiller, A.: The Bluelink ocean data assimilation system (BODAS), *Ocean Modelling*, 21, 46–70, 2008.



- Powell, B. S. and Moore, A. M.: Estimating the 4DVAR analysis error of GODAE products, *Ocean Dynamics*, 59, 121–138, 2008.
- Powell, B. S., Arango, H. G., Moore, A. M., Di Lorenzo, E., Milliff, R. F., and Foley, D.: 4DVAR data assimilation in the Intra-Americas Sea with the Regional Ocean Modeling System (ROMS), *Ocean Modell.*, 25, 173–188, 2008.
- Powell, B. S., Janekovic, I., Carter, G. S., and Merrifield, M. A.: Sensitivity of Internal Tide Generation in Hawaii, *Geophys. Res. Lett.*, in press, 2012.
- Puri, K., Dietachmayer, G., Steinle, P., Dix, M., Rikus, L., Logan, L., Naughton, M., Tingwell, C., Xiao, Y., Barras, V., Bermous, I., Bowen, R., Deschamps, L., Franklin, C., Fraser, J., Glowacki, T., Harris, B., Lee, J., Le, T., Roff, G., Sulaiman, A., Sims, H., Sun, X., Sun, Z., Zhu, H., Chattopadhyay, M., and Engel, C.: Operational implementation of the ACCESS Numerical Weather Prediction system, *Australian Meteorological and Oceanographic Journal*, 63, 265–284, 2013.
- Ridgeway, K. and Hill, K.: The East Australian Current, A Marine Climate Change Impacts and Adaption Report Card for Australia 2009, NCCARF Publication, 2009.
- Ridgway, K. and Godfrey, J.: Seasonal cycle of the East Australian Current, *Journal of Geophysical Research*, 102, 22 921–22 936, 1997.
- Ridgway, K., Dunn, J., and Wilkin, J.: Ocean interpolation by four-dimensional least squares -Application to the waters around Australia, *J. Atmos. Ocean. Technol.*, 19, 1357–1375, 2002.
- Roughan, M. and Morris, B.: Using high-resolution ocean timeseries data to give context to long term hydrographic sampling off Port Hacking, NSW, Australia, MTS/IEEE Kona Conference, OCEANS' 11 (Conference Paper), 6107032, 2011.
- Roughan, M., Oke, P. R., and Middleton, J. H.: A modeling study of the Climatological current field and the trajectories of upwelled particles in the East Australian current, *J. Phys. Oceanogr.*, 33, 2551 – 2564, 2003.
- Schaeffer, A., Roughan, M., Jones, E., and White, D.: Physical and biogeochemical spatial scales of variability in the East Australian Current separation zone from shelf glider measurements, *Biogeosciences Discuss.*, 12, 2015.
- Shchepetkin, A. F. and McWilliams, J. C.: Quasi-Monotone Advection Schemes Based on Explicit Locally Adaptive Dissipation, *Mon. Weather Rev.*, 126, 1541–1580, 1998.
- Shchepetkin, A. F. and McWilliams, J. C.: A method for computing horizontal pressure-gradient force in an oceanic model with a nonaligned vertical coordinate, *J. Geophys. Res.*, 108, 2003.
- Shchepetkin, A. F. and McWilliams, J. C.: The regional oceanic modeling system (ROMS): a split-explicit, free-surface, topography-following-coordinate oceanic model, *Ocean Modell.*, 9, 347–404, 2005.
- Sloyan, B. M., Ridgway, K. R., and Cowley, R.: The East Australian Current and Property Transport at 27S from 2012-2013., *J. Phys. Oceanogr.*, in press, 2016.
- Souza, J., Powell, B. S., Castillo-Trujillo, A. C., and Flament, P.: The Vorticity Balance of the Ocean Surface in Hawaii from a Regional Reanalysis, *J. Phys. Oceanogr.*, 45, 424–440, 2014.
- Stammer, D.: Global Characteristics of Ocean Variability Estimated from Regional TOPEX/ POSEIDON Altimeter Measurements, *J. Phys. Oceanogr.*, 27, 1743–1769, 1997.
- Wajsovicz, R. C.: A Consistent Formulation of the Anisotropic Stress Tensor for Use in Models of the Large-Scale Ocean Circulation, *J. Comput. Phys.*, 105, 333–338, 1993.
- Whiteway, T.: Australian Bathymetry and Topography Grid. Scale 1:5000000., Geoscience Australia, Canberra., 2009.
- Wilkin, J. L., Bowen, M. M., and Emery, W. J.: Mapping mesoscale currents by optimal interpolation of satellite radiometer and altimeter data, *Ocean Dynam.*, 52, 95:103, 2002.

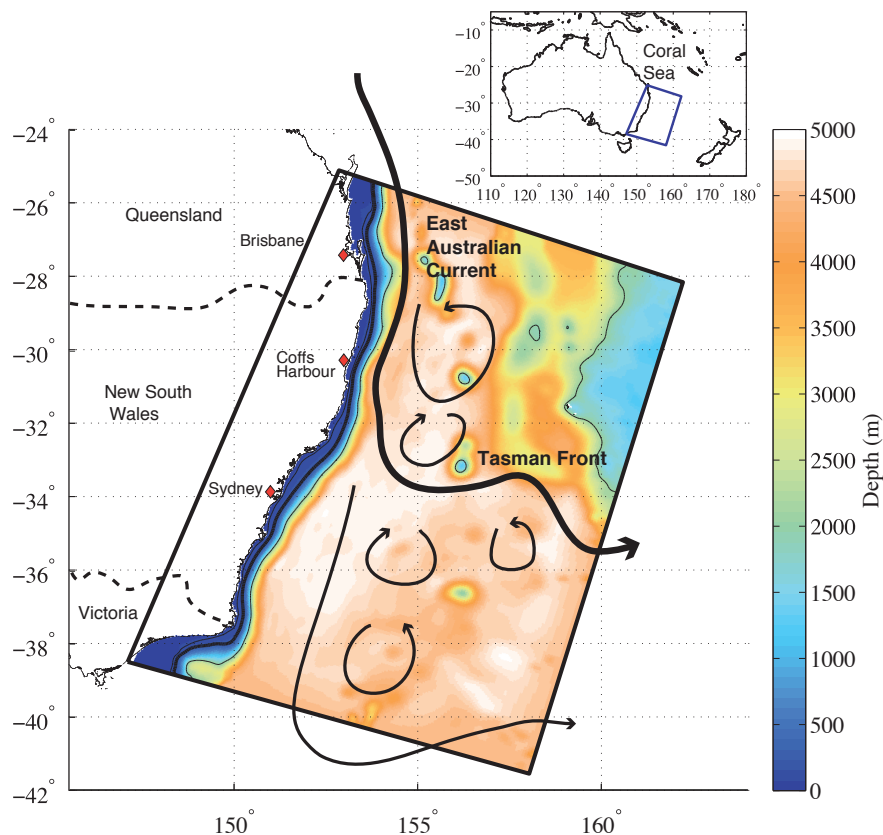


**Figure 1.** Model domain and bathymetry with the 100m, 200m (bold) and 2000m contours. Australian States are labelled and main towns are labelled and shown by the red diamonds. A cartoon of the EAC is overlain showing the typical separation latitude and the Tasman Front.

Wyatt, L. R.: Error analysis for ACORN HF radars, Integrated Marine Observing System - Australian Coastal Ocean Radar Network, ACORN report 2014-2, 2014.

Zavala-Garay, J., Wilkin, J. L., and Arango, H. G.: Predictability of mesoscale variability in the East Australian Current given strong-constraint data assimilation, *Journal of Physical Oceanography*, 42, 1402–1420, 2012.

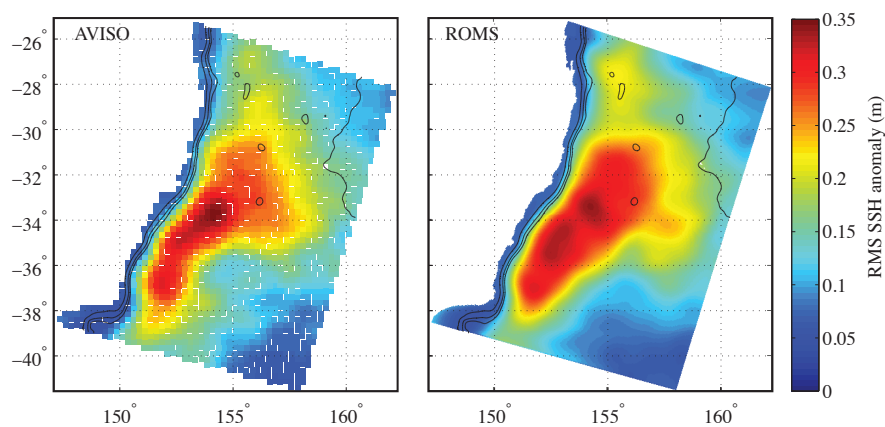


**Figure 2.** Root mean squared (RMS) SSH anomaly over 10 year period from AVISO (left panel) and ROMS 10yr free run (right panel).

**Table 1.** Total full-water-column alongshore transport (Sv) through 27.5° S (EAC deep water array), 30.3° S (Coffs Harbour) and 33.9° (Sydney) cross-shore sections as shown in Figure 3, computed daily for the 10-year free-running model period.

<b>Transport (Sv)</b>		
<b>EAC Array (27.5° S)</b>	mean	-14.3
	std	28.4
	min	-97.9
	max	59.5
<b>Coffs Harbour (30.3° S)</b>	mean	-21.9
	std	31.7
	min	-120.2
	max	66.5
<b>Sydney (33.9° S)</b>	mean	-6.9
	std	39.2
	min	-163.0
	max	117.8

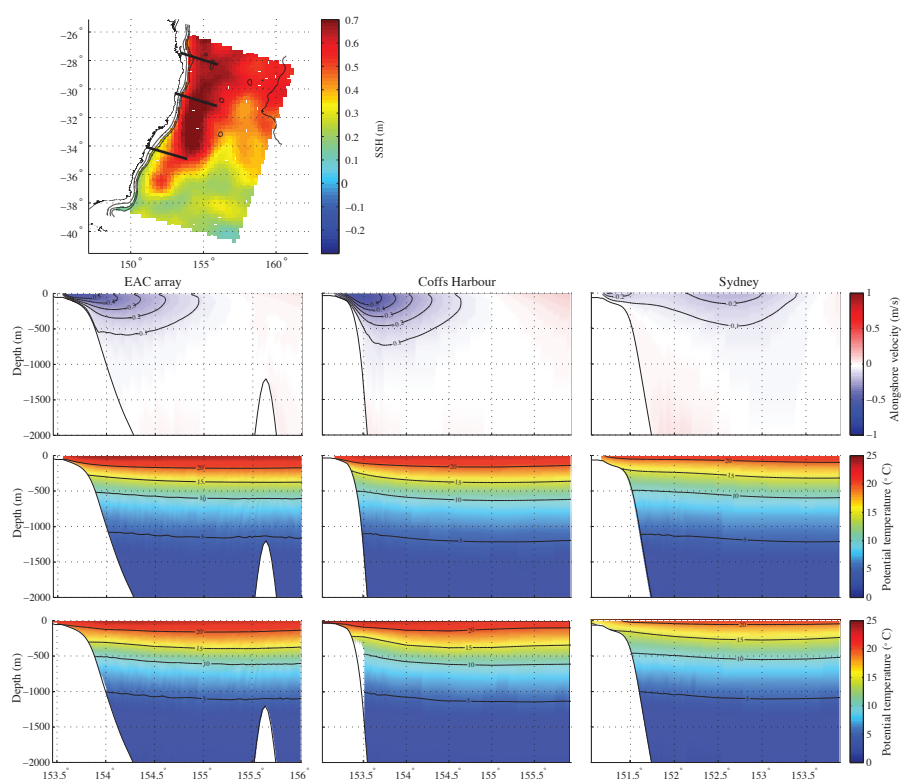


**Figure 3.** Mean SSH from AVISO showing cross-shore sections that cross the coast at the EAC Transport array (27.5° S), Coffs (30.3° S) and Sydney (33.9° S), top panel. Mean alongshore velocity from the ROMS 10yr free run at the respective cross-shore sections, top row, mean temperature from the ROMS 10yr free run, middle row, and mean temperature from CARS climatology, bottom row.

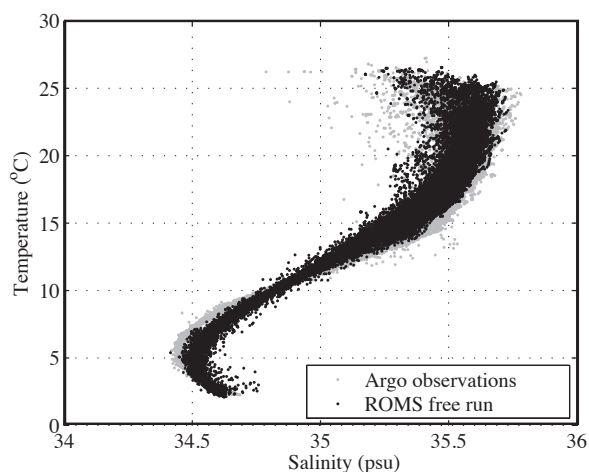


**Figure 4.** Temperature-Salinity diagram for the Argo observations and corresponding values from the 2yr free run for 2012-2013.

**Table 2.** Mooring information for the EAC deep water array moorings (EAC1-5), South East Queensland shelf moorings (SEQ200, SEQ400) and the NSW shelf moorings (CH100, SYD100, SYD140).

Name	Lat (° S)	Lon (° E)	Water depth (m)	Distance offshore (km)	Temporal coverage	Sensor Depth Range (m)		
						Temperature	Salinity	Velocity
CH100	30.27	153.40	98	25	1 Jan 2012 - 30 Dec 2013	5-100	-	9-89
SYD100	33.94	151.38	104	10	1 Jan 2012 - 30 Dec 2013	11-107	-	1-99
SYD140	33.99	151.45	138	19	1 Jan 2012 - 30 Dec 2013	21-143	-	24-129
EAC1	27.31	153.97	1525	53	21 Apr 2012 - 23 Aug 2013	60-1060	60-1060	43-1054
EAC2	27.31	153.99	1940	55	22 Apr 2012 - 24 Aug 2013	163-1045	163-1045	9-1495
EAC3	27.25	154.29	4220	85	23 Apr 2012 - 24 Aug 2013	156-3991	156-3991	9-3968
EAC4	27.21	154.65	4745	121	25 Apr 2012 - 25 Aug 2013	154-4009	154-4009	38-3974
EAC5	27.10	155.30	4797	185	26 Apr 2012 - 26 Aug 2013	192-1109	192-1109	107-4016
SEQ400	27.33	153.88	405	44	01 Apr 2012 - 06 Jun 2013	48-375	48-375	23-405
SEQ200	27.34	153.77	209	33	01 Apr 2012 - 06 Jun 2013	40-189	40-189	23-196

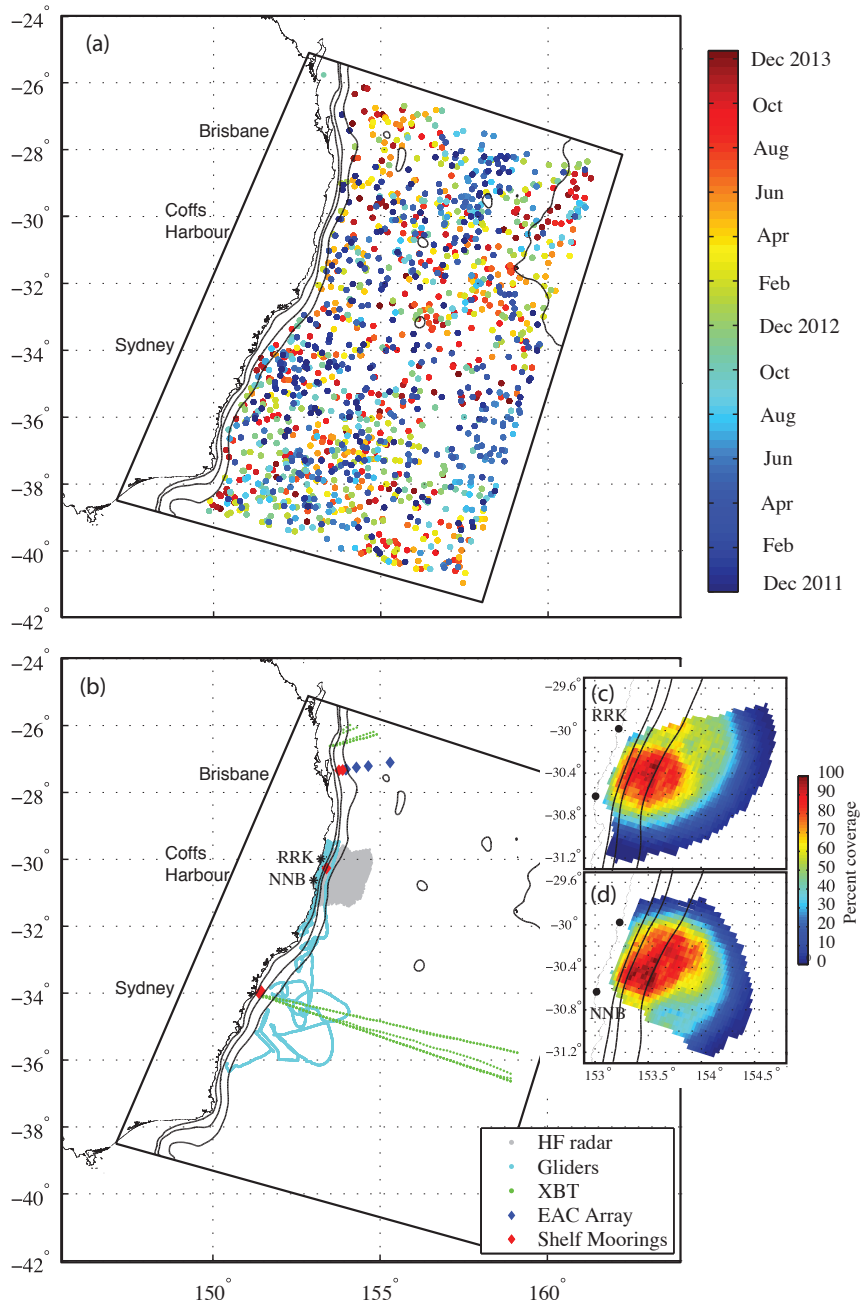


**Figure 5.** Argo observations coloured by time of occurrence, (a), and all other observations, with the exception of satellite-derived SSH and SST, (b). 100m, 200m and 2000m contours are shown. Coastal towns are labelled in line with their location on the coast. HF radar sites Red Rock (RRK) and North Nambucca (NNB) are shown with black asterisks in (b) and zooms showing the percent coverage of radial data for the two stations are shown in (c) and (d).

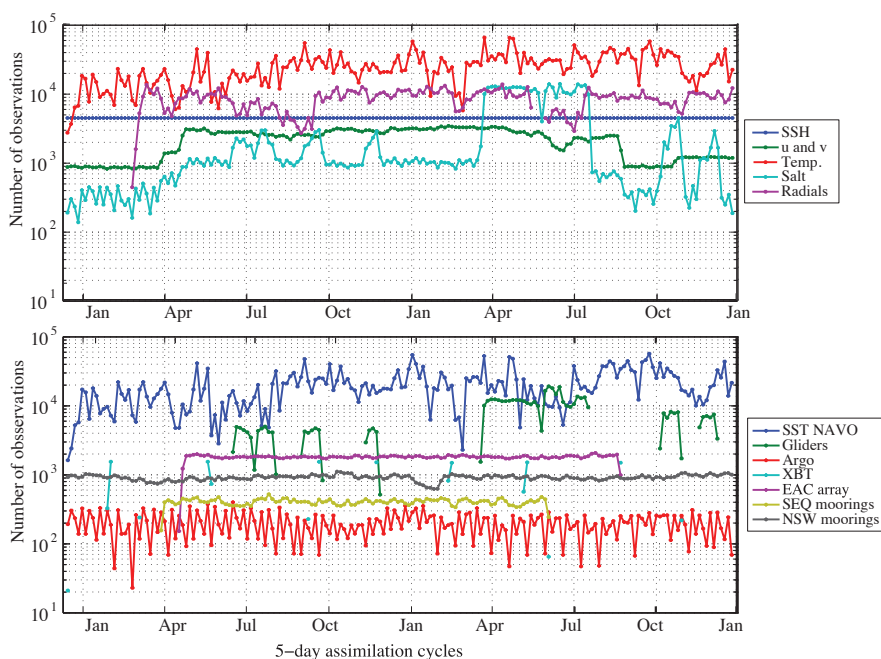


**Figure 6.** Number of observations (after processing) used in each 5-day assimilation window; for each observation type, (a), and temperature observations for each data source, (b).

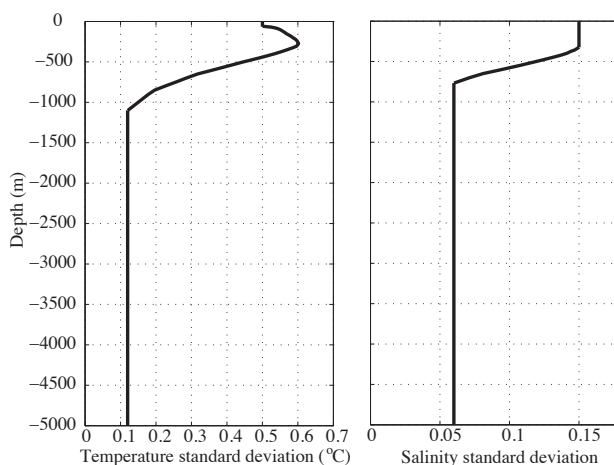


**Figure 7.** Nominal minimum observation uncertainty profiles applied to subsurface temperature and salinity observations offshore of the continental shelf.

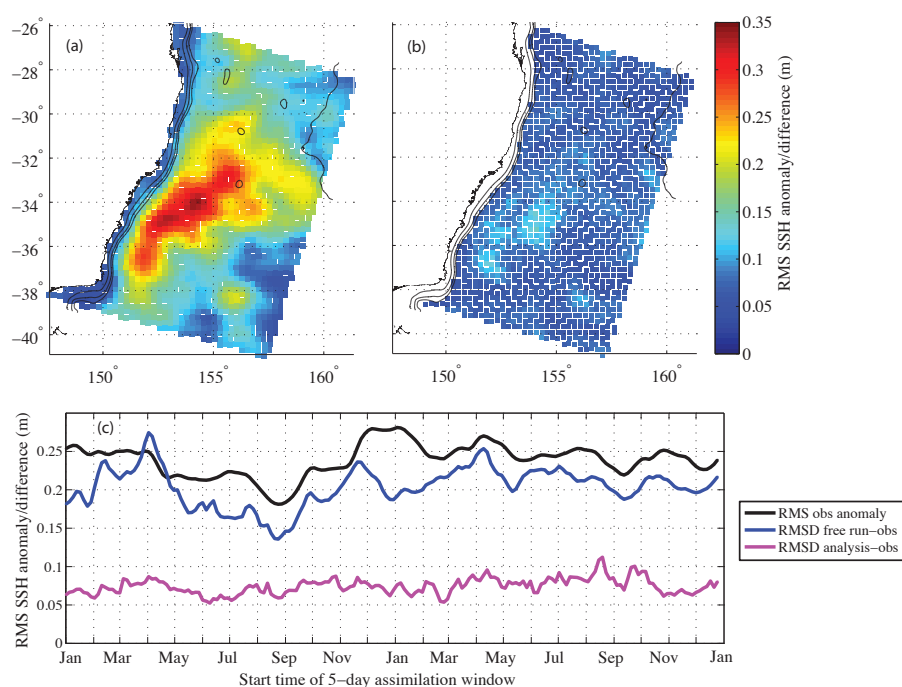


**Figure 8.** RMS SSH observation anomaly (a) and RMS SSH difference between the analysis and observations (b) for the 2-year assimilation window. Time-series of spatially-averaged RMS SSH observation anomaly, RMS SSH difference between the free run and observations, and RMS SSH difference between the analysis and observations, for each assimilation window (c).

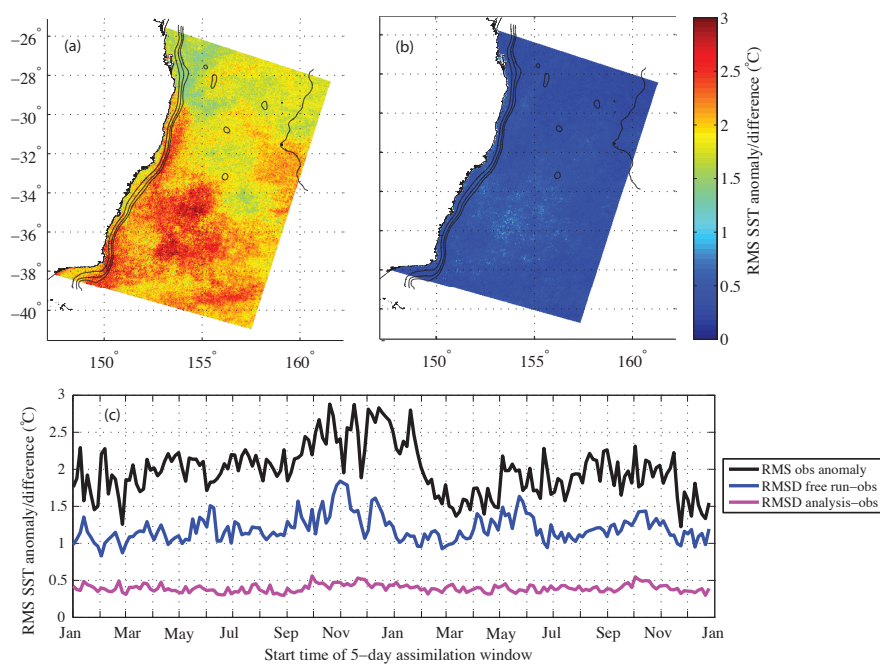


**Figure 9.** RMS SST observation anomaly, including seasonal cycle, (a) and RMS SST difference between the analysis and observations (b) for the 2-year assimilation window. Time-series of spatially-averaged RMS SST observation anomaly, RMS SSH difference between the free run and observations, and RMS SSH difference between the analysis and observations, for each assimilation window (c).

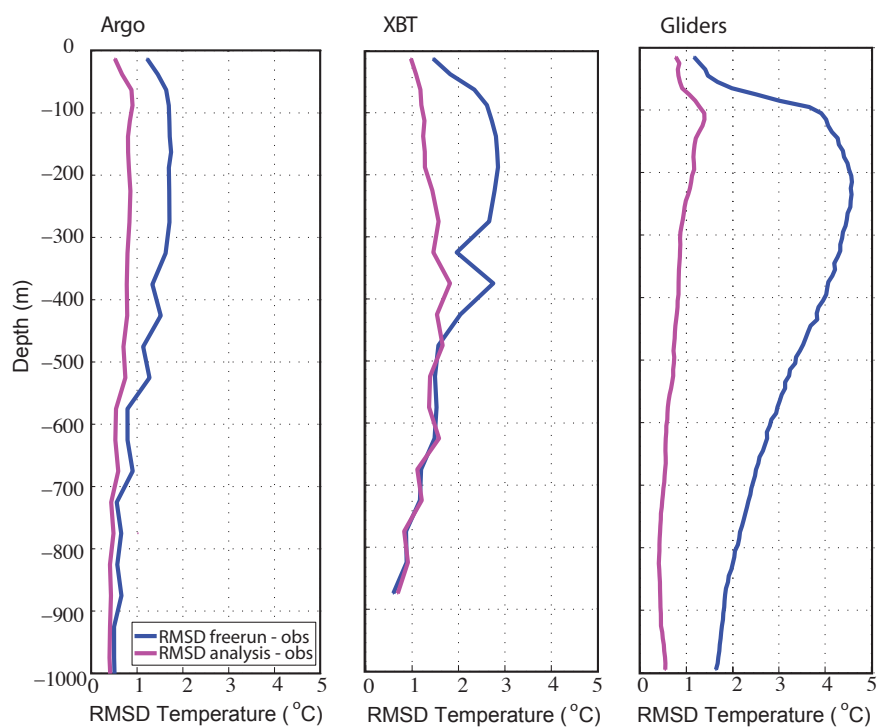


**Figure 10.** RMS difference between the free run and observations, and the analysis and observations for Argo (a), XBT (b) and Glider (c) observations in nominal depth bins for the 2-year assimilation window. Argo and XBT depth bins are 25m from the surface to 200m and 50m below 200m, Glider bins are 10m throughout the water column.

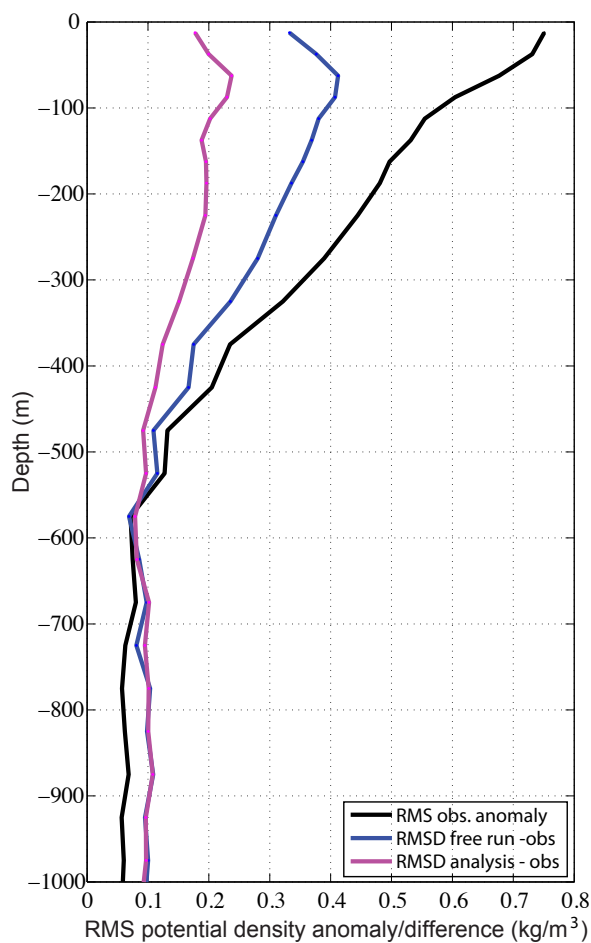


**Figure 11.** RMS potential density observation anomaly and RMS difference between the free run and observations, and the analysis and observations for Argo float observations. Observations are grouped into nominal depth bins of 25m from the surface to 200m and 50m below 200m.

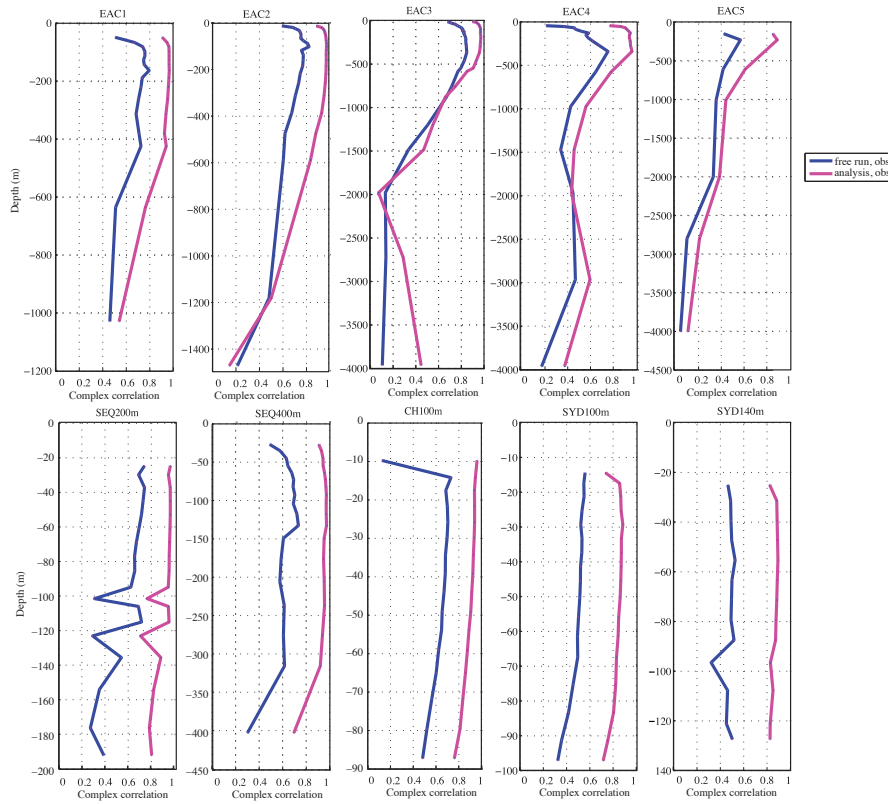


**Figure 12.** Complex correlation between observed velocities and free run and analysis velocities at mooring locations.

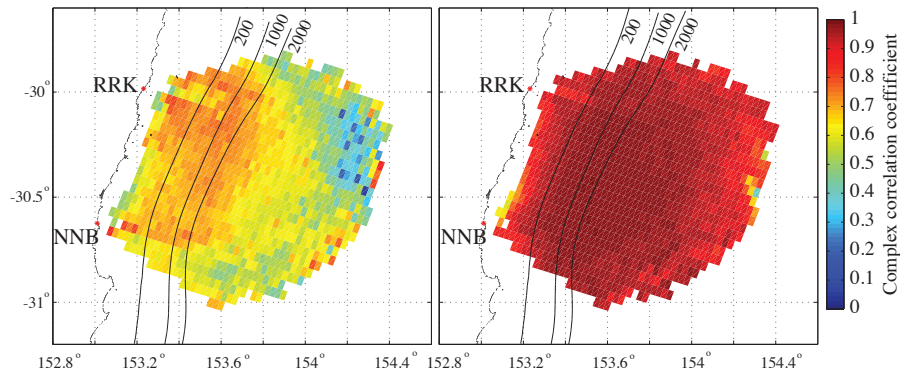


**Figure 13.** Complex correlation of surface velocities computed from the assimilated HF radar radials, and surface velocities computed from the corresponding free run (left) and analysis (right) radials. 200m, 1000m and 2000m bathymetry contours are shown.

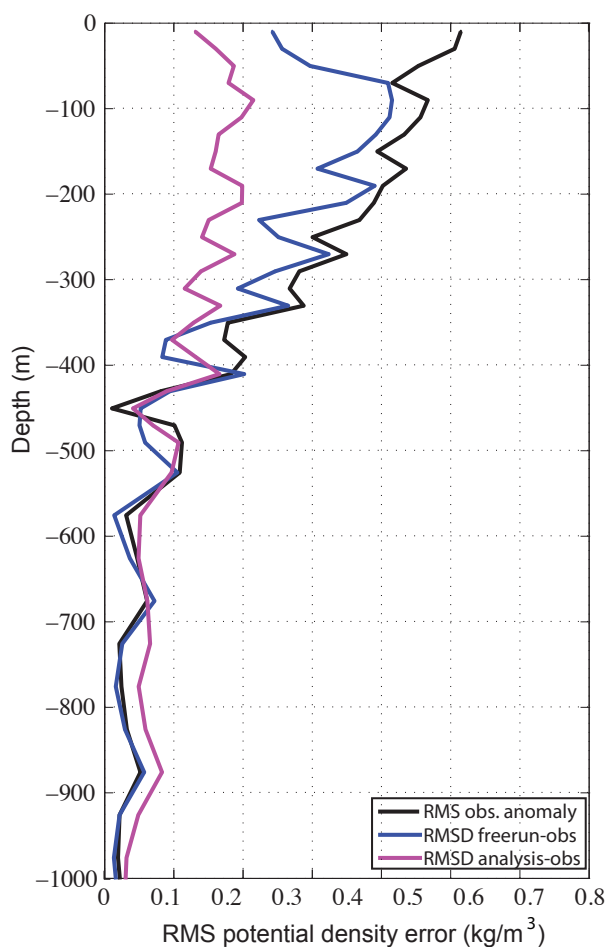


**Figure 14.** RMS potential density observation anomaly and RMS difference between the free run and observations, and the analysis and observations for independent CTD cast observations mapped to model vertical levels. Observations are grouped into nominal depth bins of 20m from the surface to 500m depth and 50m below 500m.